Published in Review of Scientific Instruments 83, issue 10, 104706-1/8, 2012
which should be used for any reference to this work

Compact microwave cavity for high performance rubidium frequency standards

Camillo Stefanucci,[1,a)] Thejesh Bandi,[2,a)] Francesco Merli,[1] Matthieu Pellaton,[2] Christoph Affolderbach,[2] Gaetano Mileti,[2] and Anja K. Skrivervik[1]
[1]*Laboratoire d'Électromagnétisme et d'Acoustique (LEMA), École Polytechnique Fédérale de Lausanne, CH-1015 Lausanne, Switzerland*
[2]*Laboratoire Temps-Fréquence (LTF), Institut de Physique, Université de Neuchâtel, CH-2000 Neuchâtel, Switzerland*

The design, realization, and characterization of a compact magnetron-type microwave cavity operating with a TE_{011}-like mode are presented. The resonator works at the rubidium hyperfine ground-state frequency (i.e., 6.835 GHz) by accommodating a glass cell of 25 mm diameter containing rubidium vapor. Its design analysis demonstrates the limitation of the loop-gap resonator lumped model when targeting such a large cell, thus numerical optimization was done to obtain the required performances. Microwave characterization of the realized prototype confirmed the expected working behavior. Double-resonance and Zeeman spectroscopy performed with this cavity indicated an excellent microwave magnetic field homogeneity: the performance validation of the cavity was done by achieving an excellent short-term clock stability as low as $2.4 \times 10^{-13}\ \tau^{-1/2}$. The achieved experimental results and the compact design make this resonator suitable for applications in portable atomic high-performance frequency standards for both terrestrial and space applications.

I. INTRODUCTION

Rubidium (Rb) atomic clocks[1,2] are used as secondary frequency standards. Their compactness and competitive stability—over one to several days—make them interesting and suitable candidates for satellite navigation and telecommunication systems applications.[3]

Most of the commercial Rb atomic clocks are based on the double-resonance (DR) spectroscopy scheme illustrated in Fig. 1 that requires two electromagnetic (EM) fields: an optical field at $\nu_{opt} = 384.23$ THz for the Rb D2-line to polarize the atoms by optical pumping, and a microwave field at ν_{Rb} (unperturbed value[4] equals to 6 834 682 610.90 429(9) Hz) to drive the ground-state hyperfine clock transition that serves as atomic frequency reference.

Cylindrical,[5] rectangular,[6] or mixed-design microwave cavities[7] are usually used to apply the microwave field to the Rb atoms contained in vapor form inside a glass cell. In order to achieve a compact design fulfilling the electromagnetic requirements for our application,[8] the loop-gap resonator (LGR)[9] was selected as a first model. This typology has a broad field of applications including electron spin resonance (ESR),[10] electron paramagnetic resonance (EPR),[9] and nuclear magnetic resonance (NMR)[11] as it provides excellent EM characteristics within a volume three times more compact than a simple cylindrical cavity.

The microwave magnetic field distribution of the LGR, also named split-ring or slotted-tube resonator,[12,13] is interesting for frequency standards application where it is known as magnetron cavity.[14] Examples in portable ground and space atomic clocks include the rubidium atomic frequency standard (RAFS), where the cavity holds a vapor cell of 14 mm diameter and resonates at 6.835 GHz,[14,15] and the passive hydrogen maser (PHM)[16] accommodating a hydrogen storage bulb of ∼60 mm diameter and resonating at 1.42 GHz.

This work focuses on a compact magnetron cavity to guarantee a clock signal with an improved short term stability better than the conventional RAFS and PHMs.[17] Recently, the stability of atomic vapor cell standards has been improved by the use of lasers for state preparation.[1,18–20] The short-term frequency stability of a clock (in terms of Allan deviation) is inversely proportional to the atomic quality factor and to the signal-to-noise (S/N) ratio.[5] This implies that a narrow linewidth of the atomic clock signal increases the atomic quality factor and thereby improves the short-term clock stability. A larger dimension of the rubidium cell results in a higher atomic quality factor and allows interrogating more atoms with the standing microwave field, and hence, gives a better S/N ratio. Previous studies were done on magnetron-type cavity that can accommodate 14 mm diameter cells, whereas here we develop and study a larger cavity that can hold an enlarged cell of 25 mm diameter.

To summarize, this paper focuses on the design of a resonator for enlarged Rb cells while still ensuring the compactness of the overall system (LGR cavity).

The manuscript is organized as follows: Sec. II describes the LGR model and the design of the magnetron cavity which resonates around ν_{Rb} in a TE_{011}-like mode. Analytical and numerical investigations are carried out in order to evaluate the limitations of the lumped elements equivalent model and to compute the performance of the cavity. This is followed by the simulated and experimental microwave characterization of the resonator in Sec. III. The field mode analysis of the designed magnetron cavity in double-resonance spectroscopic

[a)]C. Stefanucci and T. Bandi contributed equally to this work.

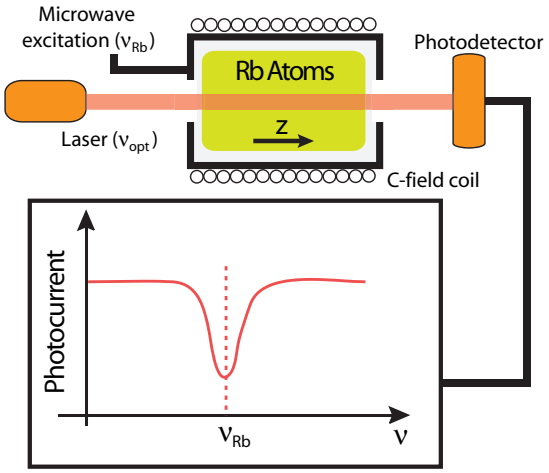

FIG. 1. DR spectroscopy principle: Rb atoms inside a cell are excited by a laser beam at ν_{opt} and an EM field at ν_{Rb}. The clock frequency is determined by a photodetector. The C-field is a dc magnetic field to separate the hyperfine energy levels by Zeeman splitting[5] and it identifies the quantization axis[1] (it coincides with the z-axis).

experiments is presented in Sec. IV. Finally, Sec. V validates the cavity by demonstrating the frequency stability of our clock, while conclusions are drawn in Sec. VI.

II. MICROWAVE CAVITY DESIGN

A. Loop-gap resonator model

The LGR consists in a metallic slotted loop inside a cylindrical shield. The simplicity of the structure allows the use of a lumped elements equivalent model to estimate the resonance frequency[10,21] ν_r,

$$\nu_r = \frac{1}{2\pi}\underbrace{\sqrt{\frac{n}{\pi r^2 \varepsilon \mu}\frac{t}{w}}}_{\text{LC}}\underbrace{\sqrt{1+\frac{r^2}{R^2-(r+w)^2}}}_{\text{shield}}\underbrace{\sqrt{\frac{1}{1+2.5\frac{t}{w}}}}_{\text{fringing}}, \tag{1}$$

where r is the inner loop radius, R the shield radius, n the number of gaps of thickness t, and width w as illustrated in Fig. 2(a). The three indicated terms identify the contributions of the basic inductor-capacitor (LC) equivalent circuit model, the correction due to the presence of the outer shield and the factor related to the magnetic fringing field. The corresponding resonant mode has the electric field mainly concentrated in the gaps (parallel plate capacitor), while the magnetic field is confined within the loop.[22] This mode will be named here as TE_{011}-like in analogy with cylindrical cavities, however, the transverse field distributions are different with respect to the circular geometry.

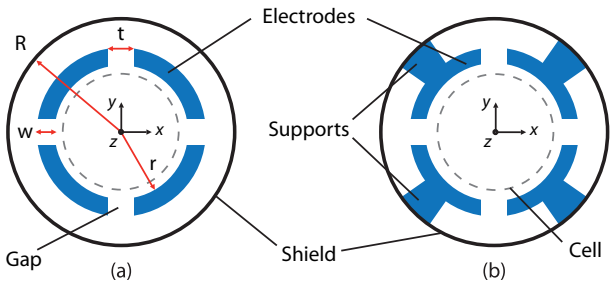

FIG. 2. Basic loop-gap resonator (a) and magnetron cross section (b) with $n = 4$ gaps. The metallic pieces and their separations are identified as electrodes and gaps, respectively. Dashed line identifies the glass cell.

Equation (1) serves as an excellent base to design a LGR, but a more precise full-wave numerical analysis is required since the lumped model does not take into account the following aspects:

(a) The dielectric cell which contains the atoms in the vapor form.
(b) The metallic supports which attach the electrodes to the outer shield as in a magnetron cross section,[23] Fig. 2(b).

The two aspects imply frequency shifts >3%, which are not negligible in our application.

Additionally, two other problems must be taken into account:

(a) Equation (1) does not consider the effects of the openings of the cavity required to let the laser beam interact with the Rb atoms.
(b) Equation (1) is a single mode model and thus gives no information about other excited resonances in the same frequency range of the TE_{011}-like mode.

These four issues will be further detailed in Subsections II A 1 and II A 2, highlighting the main differences between the design of small LGRs and enlarged cavities.

1. Dielectric cell and metallic supports

In order to appreciate the effect of the presence of the cell and supports, two significant examples are reported: one LGR of shield radius $R = 10.2$ mm (for a Rb cell of 14 mm diameter) and another one of $R = 18.0$ mm (for a 25 mm diameter Rb cell). Other parameters are set to obtain the targeted ν_{Rb} ($n = 4$, 6; $t = 0.841$, 2.138 mm; $w = 1.8$, 3.8 mm; $r = 7.5$, 13.5 mm; $R = 10.2$, 18 mm, for the two cases, respectively).

The relative errors between the resonant frequencies of the TE_{011}-like mode of real structures and the result of Eq. (1) are reported in Fig. 3. Four different geometries are numerically investigated with the ANSYS high frequency simulation software (HFSS):[24] basic LGR, basic LGR with a dielectric cell ($\varepsilon_r = 4.5$, thickness = 1 mm), basic LGR with supports, basic LGR with supports and dielectric cell.

Two different effects can be distinguished: while the presence of cell reduces the resonant frequency, the supports entail an upwards frequency shift. As a consequence the lumped model is shown to have an error around 10% (which can reach 25% for certain geometries). It can be noticed that the errors are more prominent for the larger cell.

2. Apertures and spurious modes

Figure 4 illustrates an LGR terminated by two open circular waveguides. These boundary conditions decrease the

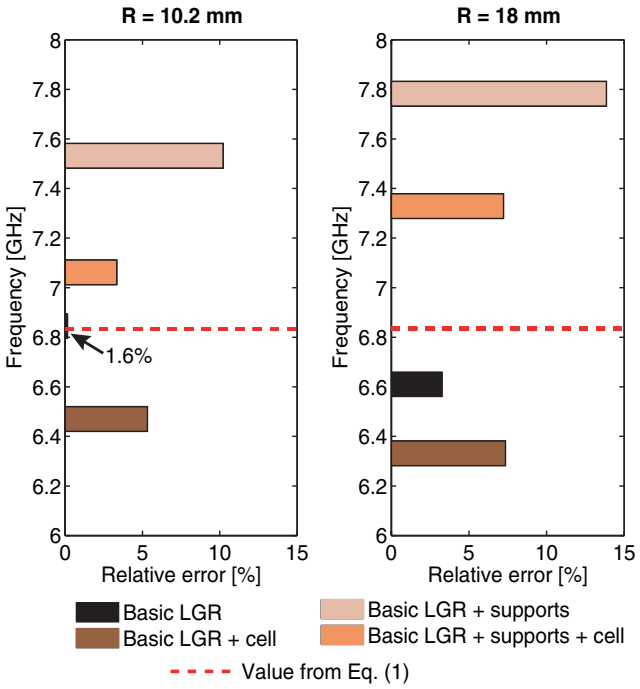

FIG. 3. Relative error of the simulated[24] eigenmode frequency of the TE_{011}-like mode with respect to the value calculated by (1) for four different geometries.

Q-factor depending on the apertures' dimensions. To understand the importance of the latter aspect when the shield diameter is increased, let us refer to the work already published by Mett.[25] In particular, the two following aspects are important to be recalled:[25]

- The central part can be modeled as a ridged circular waveguide:[25] the field distribution of the resonant frequency of LGR is as the TE_{011} mode of cylindrical resonators perturbed by the presence of the electrodes (becoming TE_{011}-like). However, other transverse modes can be excited.
- The top and bottom loading sections may support TE and TM transverse modes of a classic circular waveguide (thus, a different field distribution from the fringing configuration of the TE_{011}-like mode).

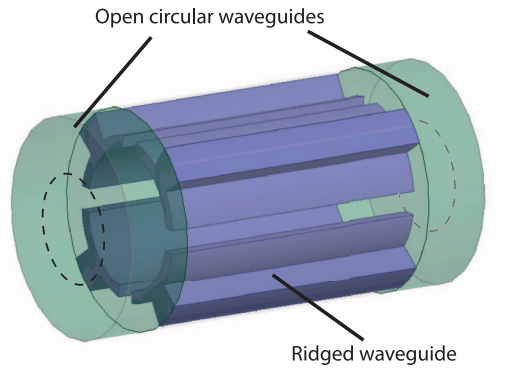

FIG. 4. Magnetron cavity model as a ridged waveguide with two circular loading waveguides. Apertures are sketched in dashed lines. The shield is not reported for clarity reason.

A full-wave analysis helps us to understand the role of apertures when the single propagating structures are considered. If a propagating mode is excited in the loading sections, it couples with the openings implying a modification of the field distribution in the central region and a stronger decrease of the Q-factor because of the related radiation. For this reason, the terminating waveguides are usually designed to work under cut-off.[10] This means for applications at ν_{Rb} setting the maximum radius of the empty circular waveguides equal to $R_c = 12.85$ mm.

In general, setting $R > R_c$ requires the precise analysis of the loading sections. Nonetheless, the previous conservative limit to the radius can be circumvented by paying a particular attention to the supported modes in the terminating circular waveguides. In fact, the TE_{01}-like transverse mode of the ridged region can propagate in the loading sectors only if $R > R_{max} = 26.75$ mm. Therefore, we can conclude that the resonant field of a LGR with an outer shield of radius $R_c < R < R_{max}$ can still be insensitive to the apertures. Obviously, the latter is also true if other modes (such as the fundamental TE_{11}) are not excited by the discontinuity between the ridged section and the loading waveguides.

The increase of R implies also the presence of more modes, which may prevent the correct functioning of the Rb atomic clock. Indeed, a field distribution with transverse magnetic components H_t drives unwanted σ Zeeman transitions[26] (see Sec. IV B).

Table I reports the relative frequency difference of the TE_{011}-like mode and the closest resonant mode with consistent H_t. It is evident that for the larger cavity the modes are closer in frequency, and the combination of the described effects can lead to undesirable configurations where both modes overlap ($\Delta f < 5\%$). It is worth reminding that this situation can pose problem for tuning of the cavity and the correct functioning of the clock.

B. Magnetron cavity design

After a first estimation of the geometrical dimensions via Eq. (1), a magnetron cavity with six electrodes was designed. Iterative optimization procedure was performed to include all the details of the final realization into the numerical simulations. The proposed structure is depicted in Fig. 5. A coaxial cable loop placed under the middle of the electrodes excites

TABLE I. Relative frequency difference $\Delta f = (f_{TE} - f_{H_t})/f_{TE}$ between the simulated TE_{011}-like mode (f_{TE}) and the first H_t mode (f_{H_t})[a] for the same geometries of Fig. 3.

$R = 10.2$ mm	Basic	+Cell	+Suppression	+Cell + suppression
f_{TE} (GHz)	6.845	6.496	7.532	7.062
f_{H_t} (GHz)	7.495	5.321	8.676	7.906
$\lvert\Delta f\rvert$	9.5%	17.7%	15.2%	11.9%
$R = 18$ mm	Basic	+Cell	+Suppression	+Cell + suppression
f_{TE} (GHz)	6.610	6.333	7.782	7.329
f_{H_t} (GHz)	6.147	7.163	7.751	7.121
$\lvert\Delta f\rvert$	7.0%	13.1%	3.1%	2.84%

[a]Notice that f_{H_t} is the closest H_t mode for each investigated case.

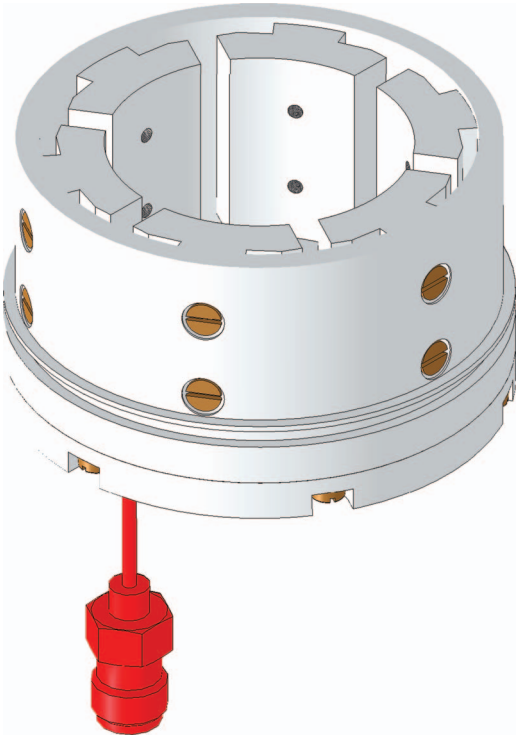

FIG. 5. Computer-aided-design (CAD) of magnetron cavity with six electrodes and a coaxial excitation. The closing cap is not reported to appreciate the electrodes shape.

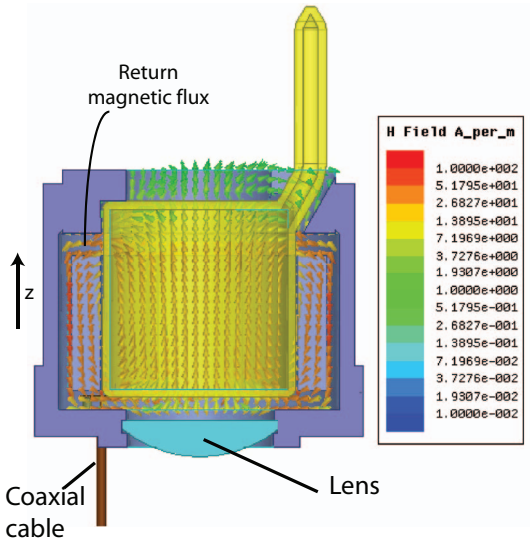

FIG. 6. Simulated H-field distribution at 6.835 GHz (side cut) with an input power of 1 W. The analysis includes the semi-rigid coaxial cable loop, the optical lens needed to focus the light onto a photodetector and the glass cell.

the cavity and ensures a good coupling[27] with the desired TE_{011}-like mode. The shield, $R = 18$ mm, and the electrodes allow the insertion of a glass cell of 25 mm in diameter. The latter can be precisely positioned with a metal cap inserted into the cavity; this mechanism allows also the fine tuning of the resonator at 6.835 GHz within a 200 MHz range (<3%).[15]

III. MICROWAVE CAVITY CHARACTERIZATION

A. Simulated performances

The simulated microwave magnetic field distribution of the proposed magnetron cavity is reported in Fig. 6. The H-field distribution of the TE_{011}-like mode is uniform along the z-direction with small radial and azimuthal components. It is important to notice that the difference between the resonance frequency predicted by (1) and the full wave numerical analysis is larger than 25% including all the geometrical details of the final design.

To characterize the microwave magnetic field distribution for DR frequency standards, we considered the filling factor $\eta\prime$ and the field orientation factor ξ.

The filling factor—mainly used in the context of active hydrogen masers—is defined as[5]

$$\eta' = \frac{1}{V_{\text{cell}}} \frac{(\int_{V_{\text{cell}}} H_z dV)^2}{\int_{V_{\text{cavity}}} |\mathbf{H}|^2 dV}, \tag{2}$$

where V_{cell} is the volume occupied by Rb atoms (excluding the reservoir) and V_{cavity} is the total volume of the cavity inside the shield including the cell. The z-direction here is supposed to coincide with the direction of the static magnetic C-field defining a quantization axis and it is parallel to the light propagation direction[1] as shown in Fig. 1. Thus, $\eta\prime$ measures the fraction of magnetic field energy useful for the clock signal (H_z drives the ground-state clock transition as detailed in Sec. IV) compared to the total microwave energy stored in the cavity. It is a measure of the efficiency of the cavity for coupling the overall microwave energy to the atoms stored in the cell, which is an important parameter for an active hydrogen maser.

In the case of a passive Rb vapor-cell clock it is helpful to evaluate the homogeneity of the H-field orientation across the cell volume. In order to optimize the fraction of the magnetic field component useful for driving the clock transition with respect to the total field energy over the cell volume, we define the field orientation factor (FOF) ξ as

$$\xi = \frac{\int_{V_{\text{cell}}} H_z^2 dV}{\int_{V_{\text{cell}}} |\mathbf{H}|^2 dV}, \tag{3}$$

where the z-axis is chosen as above. As for η', the maximum value of ξ is 1 which implies the absence of the σ Zeeman transitions (H-field is exclusively z-oriented in this case). Note, that in contrast to $\eta\prime$, the value of ξ does not depend on the ratio of the cell and the cavity volumes. Thus, ξ measures the proportion of the useful magnetic field (parallel to the C-field and the light) to the total field in the cell. For completeness, note that ξ is a good estimator of the DR signal quality for buffer gas cells, where the alkali atoms can be treated as localized in space (on the timescales relevant for the DR signal).

The performances of the proposed magnetron cavity are reported in Table II. One can appreciate the high ξ value >0.85, while the filling factor (0.136) is more than two times less than the optimum value achievable in cylindrical resonators[8] (0.36) for the chosen cell dimensions.

TABLE II. Simulated microwave performance of the proposed magnetron cavity.

Parameter	Symbol	Value
Resonant frequency (GHz)	f_r	6.831
Filling factor	$\eta\prime$	0.136
Field orientation factor	ξ_{sim}	0.877
Volume (dm^3)	V_{cavity}	0.044
Q-factor (unloaded)[a]	Q_{o}	488
Q-factor (loaded)[b]	Q_{l}	185

[a]From eigenmode simulation.
[b]Excitation, holes, and reservoir included.

As a matter of fact, $\eta\prime$ can be improved increasing the return flux cross-section, see Fig. 6, at the price of a larger shield radius.[9] Our design focused on the compactness of the structure, which provides an excellent working behavior because of its high ξ as shown in Sec. V. The resonator cavity has a compact volume of <0.045 dm^3 (with a cell of 0.012 dm^3), in comparison to a TE$_{011}$ cylindrical cavity that would have a volume of $\simeq$0.14 dm^3.

Finally, the loaded Q-factor ($Q_{\text{l}} < 200$) meets the passive atomic clocks requirements[5] and ensures a negligible cavity pulling contribution on the atomic signal.[28] Q_{l} is less than half the value of the unloaded Q-factor because of the presence of the apertures for the optical interaction.

B. Measured characteristics

The realized microwave cavity is illustrated in Fig. 7. The different pieces are made of surface treated aluminum and assembled using brass screws. A borosilicate glass cell contains Rb vapor and buffer gases.[5] A 50 Ω semi-rigid coaxial cable is used to obtain the desired loop excitation.

The microwave characterization was performed with a vector network analyzer (VNA) HP8720D. The cap and the cell were screwed into the cavity to fine tune the resonator at 6.835 GHz. Two different effects are induced: first, the dielectric loading due to the glass cell reduces f_r and, second, the perturbation of the fringing field by the metal cap results in an upward f_r shift. As the cap approaches the electrodes (<4 mm), the latter effect becomes predominant.

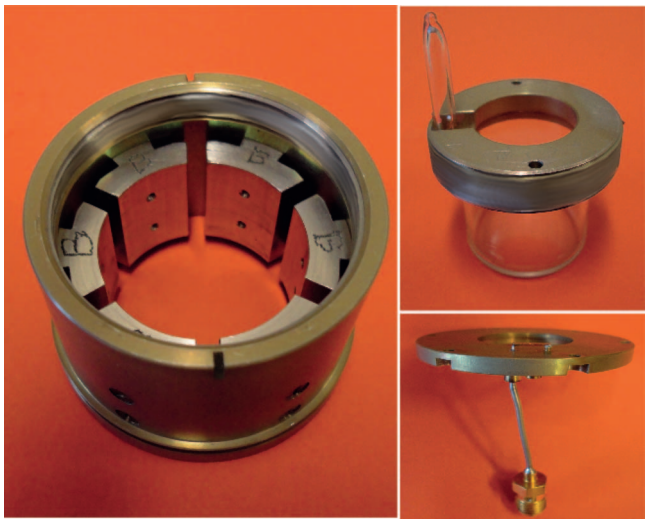

FIG. 7. Realized prototype (left). The tuning front cap attached to the cell and the coupling loop attached to the bottom enclosure are detailed on the right.

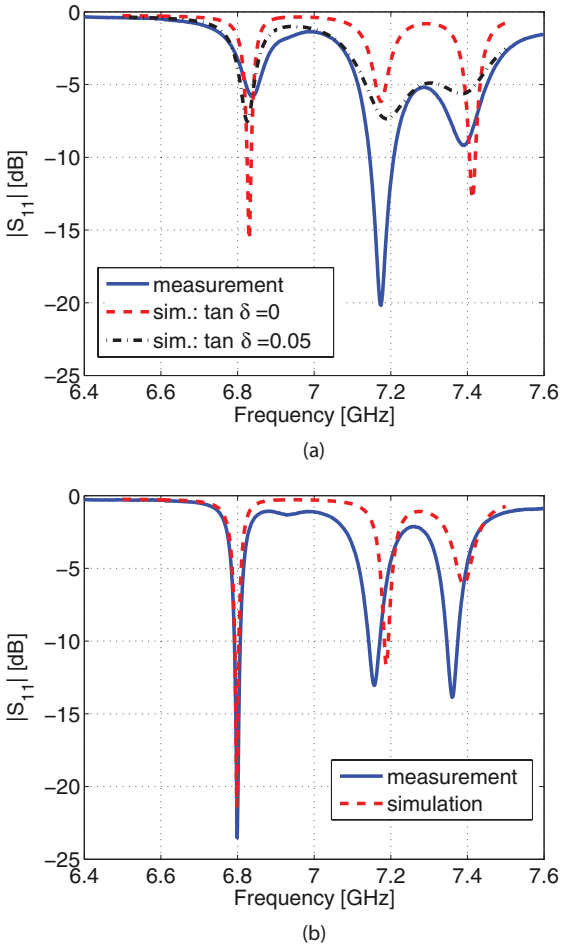

FIG. 8. Measured and simulated $|S_{11}|$ of the proposed magnetron cavity: (a) glass cell filled with rubidium thermal vapor in the tuned configuration; (b) glass cell filled with air (for a slightly different tuning).

Simulated and experimental performances are reported in Fig. 8(a). An agreement within 3% is noticed regarding the resonance frequencies, while a less close matching is observed in terms of the amplitude of the reflection coefficient $|S_{11}|$. Experimental and numerical evidence suggests that this discrepancy may be due to the presence and the modeling of the Rb vapor and any remaining Rb in liquid phase. As reported in Fig. 8(b), the simulated and experimental results are almost superimposed when considering an empty cell (Rb as free space).

On the contrary, when considering the Rb vapor as lossy material (loss tangent $\tan\delta = 0.05$), numerical results match the measured performance at 6.835 GHz as shown in Fig. 8(a). However, further investigation is required with regard to this phenomenon.

Finally, two other resonating modes at $\nu = 7.17$, 7.41 GHz are noticeable, which are not overlapping with the TE$_{011}$-like mode at ν_{Rb} ($\Delta f \geq 5\%$).

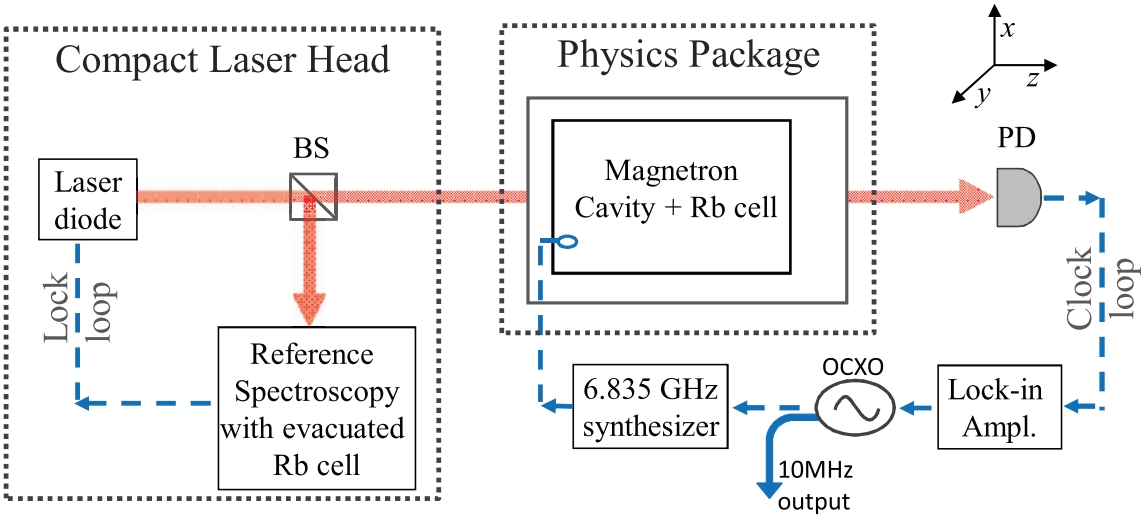

FIG. 9. Clock experimental setup showing the laser head module used for stabilizing the laser, the physics package module containing the Rb cell inside a magnetron resonator, and the clock loop with the OCXO oscillator and microwave synthesizer. (BS) Beam splitter and (PD) photodetector.

IV. SPECTROSCOPIC EVALUATION OF THE MICROWAVE CAVITY

We have experimentally verified the microwave field distribution inside the resonator by microwave-optical double-resonance spectroscopy in an atomic clock configuration. The potential of the resonator is demonstrated by measurement of the clock's frequency stability in Sec. V.

A. Experimental setup

Figure 9 shows the schematics of our microwave-optical double-resonance experimental clock setup. A distributed-feedback (DFB) laser diode emitting at $\lambda_{\rm opt} = 780$ nm acts as a source to optically pump the ^{87}Rb atoms on the D2-transition ($5^2S_{1/2} \rightarrow 5^2P_{3/2}$).

An auxiliary ^{87}Rb evacuated cell is used for saturated absorption spectroscopy in order to resolve the sub-Doppler peaks.[29] A first feed-back loop stabilizes the laser frequency to a selected sub-Doppler transition, derived from this auxiliary cell. A compact laser head with a volume <0.87 dm^3 was developed based on the above principle as explained in Ref. 29. For the laser head used in this study we measured a linewidth <4.5 MHz, relative intensity noise (RIN) 7 $\times$ 10^{-14} Hz^{-1} and FM noise of 4 kHz/$\sqrt{\rm Hz}$ at 300 Hz.

The clock physics package (PP) module has an overall volume <0.8 dm^3. It contains the clock cell with a diameter of 25 mm (filled with rubidium and buffer gases), mounted inside our magnetron cavity (cf. Fig. 5) that is tuned to resonate around $\nu_{\rm Rb}$. The cell volume is heated at a temperature T_v. A dc magnetic field is applied in the direction of laser propagation (along the z-axis) using coils that are wound around the cavity. This field isolates the ^{87}Rb ground-state *clock transition* ($5^2S_{1/2}|F_g = 1, m_F = 0\rangle \rightarrow |F_g = 2, m_F = 0\rangle$) by lifting the degeneracy of the $m_F \neq 0$ Zeeman sub-levels of the ground-state hyperfine levels. The whole assembly is surrounded by a magnetic shield for suppressing fluctuations of the external magnetic field that otherwise would perturb the clock transition by second order Zeeman effects.

The microwave radiation injected into the cavity is produced by a synthesizer with a phase noise of <-108 dBrad^2/Hz at $\geq$300 Hz Fourier frequency (6.8 GHz carrier). For clock operation, a second feed-back loop established from the photodetector output to the microwave synthesizer is used to stabilize the microwave frequency to the ^{87}Rb clock transition.

B. Double resonance and Zeeman spectra

In the DR and clock experiments, the laser was stabilized to the $F_g = 2 \rightarrow F_e = 1,3$ cross-over transition[30] using the auxiliary cell. The laser intensity incident to the clock cell was about 0.6 μW/mm^2. The cell volume occupied by Rb vapor was regulated at $T_v = 333$ K. A microwave signal around 6.835 GHz with a power of -28 dBm was injected into the cavity. Under these optimized conditions, the DR signal has a narrow linewidth of 361 Hz and a contrast of 25%, see Fig. 10.

A wider span of the microwave frequency also shows DR signals due to higher Zeeman transitions with $\Delta m_F \neq 0$, as shown in Fig. 11. These σ-transitions are due to microwave magnetic field components perpendicular to the

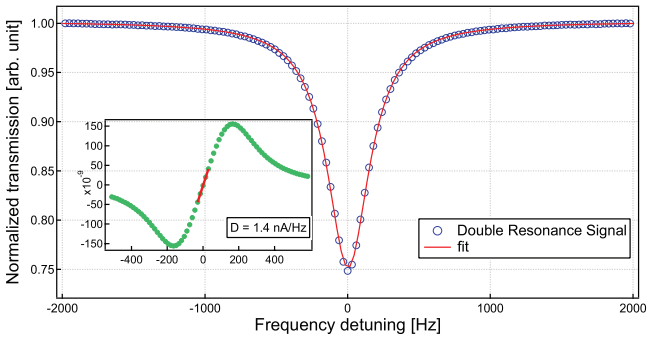

FIG. 10. Double-resonance spectroscopic signal. Inset shows the demodulated signal to which the microwave synthesizer is stabilized at the center.

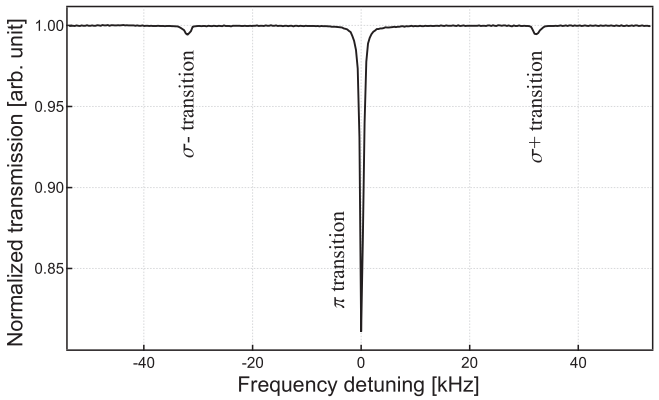

FIG. 11. Zeeman transitions for an applied C-field of 44 mG. Suppression of σ-transitions is due to TE_{011}-like H-field inside the cavity.

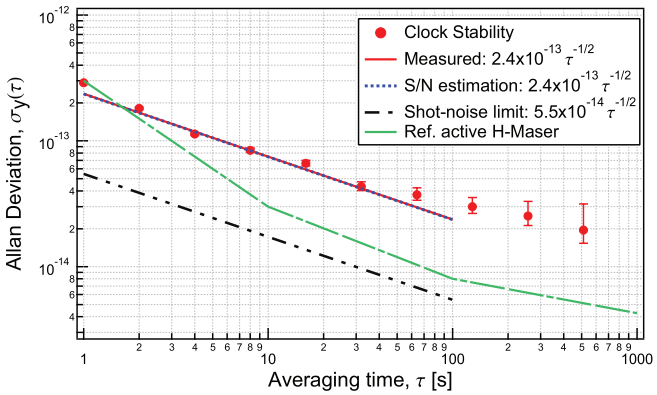

FIG. 12. Short-term clock stability. Solid line indicates the measured stability, dotted line shows the signal-to-noise estimated value, dashed-dotted line shows the shot-noise limit, and dashed line shows the stability of an active H-Maser,[32] against which the clock is measured.

z-axis (considering the static field parallel to the z-axis) and are suppressed by ∼97% compared to the central clock π-transition. The experimental field orientation factor ξ_{exp} is determined using the equation,

$$\xi_{exp} = \frac{\int S_\pi \, d\nu}{\int S_\pi \, d\nu + \int S_\sigma \, d\nu}, \tag{4}$$

where $\int S_\pi \, d\nu$ and $\int S_\sigma \, d\nu$ are the transmission signal strengths integrated with respect to the frequency detuning $d\nu$ over all the corresponding Lorentzian peaks for $\Delta m_F = 0$ (π-transitions) and $\Delta m_F = \pm 1$ (σ-transitions), respectively. For small microwave powers, the signal strengths S_π are proportional to H_z^2, and S_σ are proportional to H_t^2 (the transverse field components).[31] The value $\xi_{\rm exp} = 0.868$ computed from experimental spectra is in excellent agreement with the value estimated by simulations ($\xi_{\rm sim} = 0.877$ according to Eq. (3)). This proves that the TE_{011}-like cavity mode has a highly uniform magnetic field geometry oriented almost exclusively parallel to the laser propagating direction over the entire cell volume.

V. PERFORMANCE VALIDATION IN AN ATOMIC CLOCK

The short-term stability of a passive rubidium clock (expressed in terms of Allan deviation, $\sigma_y(\tau)$) can be predicted[19] by the equation,

$$\sigma_y(\tau) = \frac{N_{\rm psd}}{\sqrt{2} D \nu_{\rm Rb}} \tau^{-1/2}, \tag{5}$$

TABLE III. Noise budget and estimation of signal-to-noise and shot-noise limits.

Parameter	Value
FWHM	361 Hz
Contrast	25%
Discriminator	1.4 nA/Hz
$N_{\rm psd}$	3.2 pA/$\sqrt{\rm Hz}$
S/N limit	$2.4 \times 10^{-13}\ \tau^{-1/2}$
$N_{\rm shot}$	$5.5 \times 10^{-14}\ \tau^{-1/2}$

where $N_{\rm psd}$ is the total detection noise power spectral density (1 Hz bandwidth) measured when the microwave field and pump laser are switched on in a closed clock loop, $\nu_{\rm Rb}$ is the Rb ground-state hyperfine frequency, and D is the discriminator slope of the error signal close to the line center (shown in the inset of Fig. 10).

Table III summarizes the noise budget for the short-term clock stability of our setup. For the clock stability's shot-noise limit, the shot noise $N_{\rm shot}$ is calculated as $\sqrt{2eI_{\rm dc}}$, where e is the electronic charge and $I_{\rm dc} = 1.7\ \mu$A is the photocurrent of the DR signal at full width at half maximum (FWHM). For the short-term analysis of the clock stability we consider the integration time scale between 1 and 100 s.

For measurements of the clock stability, the 10 MHz output from the crystal oscillator (OCXO) (cf. Fig. 9) stabilized to the atomic clock transition is compared with a 10 MHz reference signal from an active H-Maser[32] using a frequency comparator. The clock frequency is recorded using a computer interface. The measured clock stability of $2.4 \times 10^{-13}\ \tau^{-1/2}$ is in excellent agreement with the estimated signal-to-noise limit (see Fig. 12). This stability is approximately 2 times better than the previously reported result.[19] The increase is clearly due to the improvement of the electromagnetic field distribution of the proposed cavity (i.e., high field orientation factor). We would like also to point out that this result can still be improved towards the shot-noise limit by implementing a noise-cancellation method,[33] or by using a less noisy laser source.

VI. CONCLUSION

A compact magnetron cavity for Rb frequency standards was presented. The design process started from the LRG lumped model and, showing the limitations, continued with a numerical optimization. The final prototype holds a glass cell of 25 mm and resonates with a uniform TE_{011}-like mode at $\nu_{\rm Rb}$. The simulated performances show a loaded Q-factor equal to 185, a filling factor $\eta' = 0.136$, and a new field orientation factor $\xi_{\rm sim} = 0.877$ with a volume <0.045 dm^3. Such performances ensure an excellent working behavior for the targeted application.

Microwave characterization validated the simulated analysis *albeit* experimental results suggest the necessity of further investigation about modeling of the effect of the Rb. Measured performance ($|S_{11}(\nu_{\mathrm{Rb}})| = -6$ dB) still allows clock analysis with a microwave power source as low as -28 dBm.

The suppression of σ-transitions in comparison with π-transition observed in the double-resonance experiment verified the high uniformity of the microwave magnetic field inside the cavity. This result confirms the necessity of the definition of the field orientation factor ξ (in addition to the well known filling factor) to properly characterize a resonator for Rb frequency standards. Excellent agreement is found between the simulated field orientation factor and experimentally evaluated FOF ($\xi_{\mathrm{sim}} = 0.877$, $\xi_{\mathrm{exp}} = 0.868$, respectively).

The achieved short-term clock stability of $2.4 \times 10^{-13}\ \tau^{-1/2}$ using this compact microwave cavity demonstrates better stability than that of atomic clocks presently used in satellite navigation systems,[17] such as the PHM ($6.5 \times 10^{-13}\ \tau^{-1/2}$) and RAFS ($2.5 \times 10^{-12}\ \tau^{-1/2}$). The realization of next generation portable atomic clocks using the demonstrated compact magnetron cavity for enlarged Rb cells of 25 mm diameter is thus of high interest for emerging demands in applications such as telecommunications, satellite navigation systems, local oscillators (LO) in portable optical frequency synthesizers and optical frequency standards.

ACKNOWLEDGMENTS

We acknowledge the support from the Swiss National Science Foundation (SNSF), the European Space Agency (ESA), and the Alliance and Swiss Space Office (SSO-SER). We also thank F. Gruet, P. Scherler, and M. Durrenberger from Unine-LTF, and C. E. Calosso from the Istituto Nazionale di Ricerca Metrologica (INRIM, Italy).

[1] J. Vanier and C. Mandache, Appl. Phys. B **87**, 565 (2007).
[2] J. Camparo, Phys. Today **60**, 33 (2007).
[3] G. Mileti, C. Affolderbach, F. Droz, and E. Murphy, in *ESA Bulletin* (European Space Agency, 2005), Vol. 122.
[4] S. Bize, Y. Sortais, M. S. Santos, C. Mandache, A. Clairon, and C. Salomon, Europhys. Lett. **45**, 558 (1999).
[5] J. Vanier and C. Audoin, *The Quantum Physics of Atomic Frequency Standards* (Adam Hilger, 1989).
[6] H. Williams, T. Kwon, and T. McClelland, in *37th Annual Symposium on Frequency Control* (IEEE conference publications, 1983), pp. 12–17.
[7] E. Eltsufin, A. Stern, and S. Fel, in *Proceedings of the 45th Annual Symposium on Frequency Control* (IEEE conference publications, 1991), pp. 567–571.
[8] A. Godone, S. Micalizio, F. Levi, and C. Calosso, Rev. Sci. Instrum. **82**, 074703 (2011).
[9] G. Rinard and G. Eaton, *Biomedical EPR, Part B: Methodology, Instrumentation, and Dynamics*, Biological Magnetic Resonance Vol. 24/B, edited by S. R. Eaton, G. R. Eaton, and L. J. Berliner (Springer, 2005), pp. 19–52.
[10] W. Froncisz and J. S. Hyde, J. Magn. Reson. **47**, 515 (1982).
[11] W. N. Hardy and L. A. Whitehead, Rev. Sci. Instrum. **52**, 213 (1981).
[12] T. Sphicopoulos and F. Gardiol, IEE Proc. Microwaves, Antennas Propag. H **134**, 405 (1987).
[13] B. Xia, D. Zhong, S. An, and G. Mei, IEEE Trans. Instrum. Meas. **55**, 1000 (2006).
[14] P. Rochat, H. Schweda, G. Mileti, and G. Busca, in *Proceedings of the IEEE International 48th Frequency Control Symposium (IFCS)* (IEEE conference publications, 1994), pp. 716–723.
[15] H. S. Schweda, G. Busca, and P. Rochat, U.S. patent 5,387,881 (1995).
[16] P. Berthoud, I. Pavlenko, Q. Wang, and H. Schweda, in *Proceedings of the IEEE International Frequency Control Symposium (IFCS) and PDA Exhibition Jointly with the 17th European Frequency and Time Forum (EFTF)* (IEEE conference publications, 2003), pp. 90–94.
[17] P. Waller, S. Gonzalez, S. Binda, I. Sesia, I. Hidalgo, G. Tobias, and P. Tavella, IEEE Trans. Ultrason. Ferroelectr. Freq. Control **57**, 738 (2010).
[18] G. Mileti, J. Deng, F. L. Walls, D. A. Jennings, and R. E. Drullinger, IEEE J. Quantum Electron. **34**, 233 (1998).
[19] T. Bandi, C. Affolderbach, C. Calosso, and G. Mileti, Electron. Lett. **47**, 698 (2011).
[20] S. Micalizio, C. E. Calosso, A. Godone, and F. Levi, Metrologia **49**, 425 (2012).
[21] M. Mehdizadeh and T. Ishii, IEEE Trans. Microwave Theory Tech. **37**, 1113 (1989).
[22] W. Piasecki and W. Froncisz, Meas. Sci. Technol. **4**, 1363 (1993).
[23] G. B. Collin, *Microwave Magnetrons*, MIT Radiation Laboratory Series Vol. 6 (McGraw-Hill, 1948).
[24] High frequency structure simulator (HFSS), version 13.0, 2011, see http://www.ansoft.com/products/hf/hfss/.
[25] R. Mett, J. Sidabras, and J. Hyde, Appl. Magn. Reson. **31**, 573 (2007).
[26] E. Arimondo, M. Inguscio, and P. Violino, Rev. Mod. Phys. **49**, 31 (1977).
[27] R. E. Collin, *Foundations for Microwave Engineering* (McGraw-Hill, 1966).
[28] C. Affolderbach, F. Gruet, D. Miletic, and G. Mileti, in *Proceedings of the 7th Symposium on Frequency Standards and Metrology, USA, 5–11 October 2008*, edited by L. Maleki (World Scientific, 2009), pp. 363–367.
[29] C. Affolderbach and G. Mileti, Rev. Sci. Instrum. **76**, 073108 (2005).
[30] J. Ye, S. Swartz, P. Jungner, and J. L. Hall, Opt. Lett. **21**, 1280 (1996).
[31] G. Mileti and P. Thomann, in *Proceedings of the 9th European Frequency and Time Forum (EFTF), Besançon, France, 8–10 March 1995*, edited by D. Hauden, (ACTES proceedings, 1995), pp. 271–276.
[32] R. Vessot, Metrologia **42**, S80 (2005).
[33] C. Affolderbach, F. Gruet, R. Matthey, and G. Mileti, in *Proceedings of the IEEE Frequency Control Symposium and European Frequency and Time Forum* (IEEE conference publications, 2011), p. 944.